Mixing and Turbulence in a Flooding Coastal River

Paul McKay[1]; Cheryl Ann Blain[2]; Daniela Di Iorio[3]; and Heath Hansell[4]

Abstract: An experimental study of turbulence and vertical mixing was carried out in the lower east Pearl River (Mississippi and Louisiana) during a high-discharge period in February and March of 2010. Direct estimates were made of the time-varying profile of turbulent Reynolds stresses ($\tau_x/\rho = -\overline{u'w'}$) through the water column. From this, both the vertical eddy viscosity (K_m) and mean vertical mixing time were calculated, and the water column was shown to be vertically well mixed at all times. Segmenting the stresses into stresses due to river discharge and stresses due to tidal flows shows the coequal nature of each component and highlights the ways they vary in importance during different flow regimes. Two simple turbulence models are examined and compared to the measured mixing parameters. **DOI: 10.1061/(ASCE)HY.1943-7900.0000751.** © *2013 American Society of Civil Engineers.*

CE Database subject headings: Turbulence; Water discharge; Friction; Rivers and streams; Floods; Mississippi; Louisiana.

Author keywords: Mixing processes; Turbulence; River; Discharge; Tides; Mixing length; Friction velocity.

Introduction

Rivers serve as one of the primary linkages allowing the transfer of dissolved and suspended materials and nutrients across the land margin and into the coastal ocean. Since the early work on estuarine dynamics (see, for example, Pritchard 1952, 1954; Hansen and Rattray 1965), vertical mixing, largely driven by bottom stress, has been known to be an important control on the flux of dissolved substances through its action on vertical stratification. Upstream of the estuarine zone, the effects of stratification are much diminished, and vertical mixing becomes even more effective in controlling the vertical flux of dissolved and suspended substances and especially in maintaining the suspended sediment load.

A majority of the studies of mixing in rivers have concentrated on the estuarine zone (see, for example, Peters 1997; Chant 2002; Simpson et al. 2005; Chant et al. 2007), on mixing at the river mouth (see, for example, Shteinman et al. 1993), and on mixing and entrainment in the buoyant plume (see, for example, Peters and Johns 2005). With their different physical and temporal scales, the measurement of flow and turbulence in rivers away from the estuarine zone often poses a different set of challenges (Muste et al. 2004). Most previous work has been concentrated on measuring near bed stress (see, for example, Stone et al. 2003; Liu et al. 2009) as these are the stresses that control sediment suspension and deposition. However, the use of high-frequency four-beam acoustic Doppler current profilers allows the measurement, through the variance method to be described later, of the vertical distribution of stresses throughout the water column. Thus, the vertical diffusivity both of momentum and of dissolved and suspended substances can be determined.

This paper discusses the results of a mooring experiment in the previously unstudied lower east Pearl River during a minor flood event in February and March of 2010. The study is designed to quantify the stresses throughout the water column and examine the relative influence of bottom-generated stress due to the mean river discharge, internally generated stress due to shear in the water column, and stresses due to tidal modulation of the flow as the river transitions from a high discharge regime to a more tidally influenced regime. The data gathered then further allowed the authors to evaluate some common turbulence models and assess their applicability to modeling similar tidally modulated river flows.

Study Site

The study site is the lower east branch of the Pearl River, which forms the political border between southern Louisiana and Mississippi. The Pearl River originates in central Mississippi, near the town of Edinburgh. It flows south before splitting into two channels south of Bogalusa, Louisiana. The east and west branches of the Pearl drain into Little Lake and the Mississippi Sound and eventually to the Gulf of Mexico (see Fig. 1). The Pearl River has a drainage area of approximately 22,000 km^2 (Patrick 1995) in the Pine Meadows unit of the East Gulf Coastal Plain (Thornbury 1965). The bed is generally composed of mud and sand and is periodically dredged from the study site in the Stennis Space Center buffer zone to the ocean to allow for heavy barge traffic.

Approximately 70% of the average annual rainfall of 1.72 m (Wax 1990) occurs in the winter and early spring, and flows are highest at these times. Late summer and early fall are generally characterized by low streamflows and increased tidal influence. The area is frequently affected by tropical weather, including tropical depressions, storms, and hurricanes, which can bring significant rain (Turnipseed et al. 1998), as well as high storm surge (Fritz et al. 2007).

Tidal range at the ocean boundary is as much as 1 m on spring tide and 0.3 m on neap and flows show a tidal signal with tidal

[1]Naval Research Lab, Oceanography Division, Code 7320, Stennis Space Center, MS 39529 (corresponding author). E-mail: Paul.McKay@nrlssc.navy.mil

[2]Naval Research Lab, Oceanography Division, Code 7320, Stennis Space Center, MS 39529. E-mail: Cheryl.Ann.Blain@nrlssc.navy.mil

[3]Dept. of Marine Science, Univ. of Georgia, Athens, GA 30602. E-mail: daniela@uga.edu

[4]Dept. of Marine and Environmental Systems, Florida Institute of Technology, Melbourne, FL 32901. E-mail: hhansel2009@my.fit.edu

Note. This manuscript was submitted on November 8, 2011; approved on February 25, 2013; published online on February 27, 2013. Discussion period open until May 1, 2014; separate discussions must be submitted for individual papers. This paper is part of the ***Journal of Hydraulic Engineering***, Vol. 139, No. 12, December 1, 2013. © ASCE, ISSN 0733-9429/2013/12-1213-1222/$25.00.

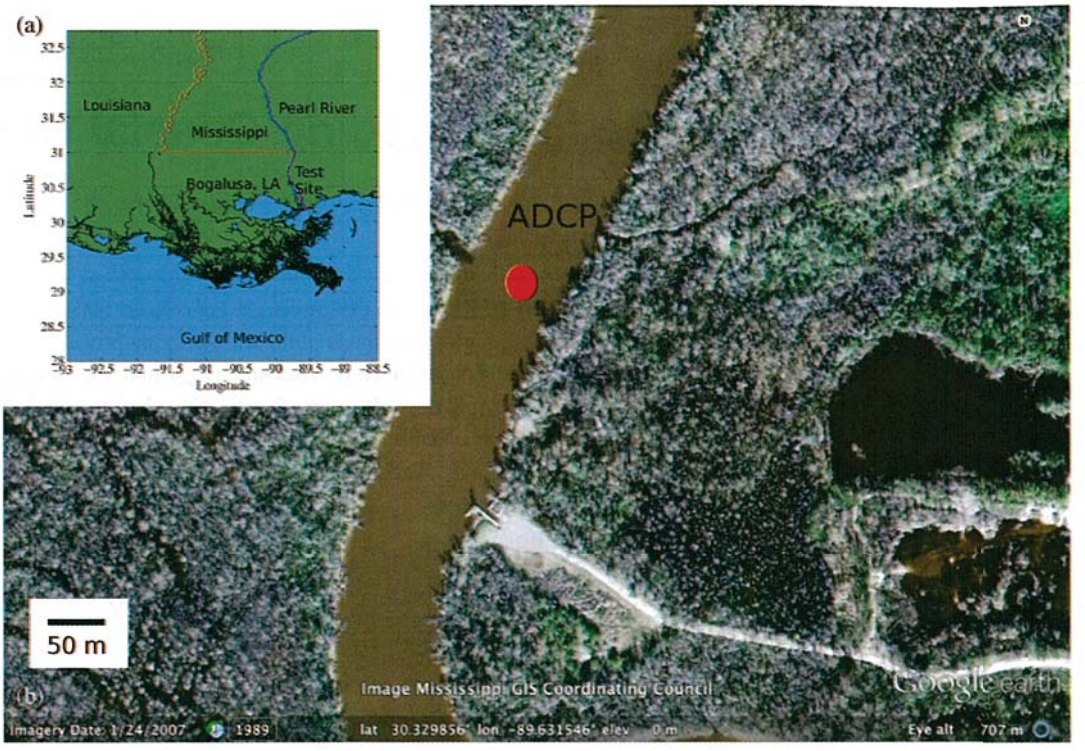

Fig. 1. (Color) Map showing the location of the lower east Pearl River and ADCP mooring; large-scale map in (a) generated using World Vector Shoreline data and aerial photograph in (b) from Google Earth, Mississippi GIS Coordinating Council

fluxes generally greater than river outflow except during high discharge events. As is typical of the north central Gulf coastal region, the dominant tidal frequency is the lunar diurnal (with a 24-h, 50-min period) on spring tide and the lunar semidiurnal (with a 12-h, 25-min period) on the (much weaker) neap tide.

The Pearl River floods frequently due to winter rains, spring runoff, and strong local storm events. Both channels of the lower Pearl are bordered by extensive floodplains, which can be significantly inundated during high-water events. At their worst, these flood events can cause significant physical and economic damage to communities on the river (Piatt 1982). Flood currents are often several times the magnitude of peak flood and ebb tidal currents and can cause extensive morphological changes to the river bed.

The study site was chosen as a straight reach of the lower east Pearl River inside of the Stennis Space Center buffer zone, where the moorings were unlikely to encounter significant vehicular traffic (see Fig. 1). Bankfull depth in the thalweg is approximately 6.75 m and bank to bank width is approximately 103 m (see Fig. 2). The east bank is lined by a natural levee that separates the river channel from a small, mostly groundwater-fed, cypress swamp. The west bank consists of marshy upland, vegetated mainly with cypress and tupelo, which divides the main channel from the Honey Island swamp. The eastern branch of the Pearl is ungauged, but discharge is generally low and tidal flows dominate during low-flow conditions, generally having peak flows of 20–50 cm/s compared to 1–2 cm/s for the tidally averaged discharge. From acoustic hydrographic surveys, the channel bed slope at this point is estimated to be approximately 1.5×10^{-4} m/m. The study site is located approximately 25 km along channel upstream of the ocean outlet and thus considerably upstream of the maximum normal extent of salt water penetration (generally 13 km from the ocean).

Experimental Program

The Pearl River mixing experiment began on February 5, 2010, at midnight GMT (Year Day 36) and ended 30 days later (Year Day 66). It was designed to allow the direct estimation of the time varying turbulent Reynolds stresses ($\tau_x/\rho = -\overline{u'w'}$), thus allowing the relative importance of vertical mixing due to sheared flow in the river considering both tidal flows and river discharge to be estimated.

The winter of December 2009 and January 2010 was unusually rainy with five times the normal amount of rain falling (approximately 65 cm) in that period in the area of New Orleans, southeastern Louisiana, and southwestern Mississippi. As a result, the lower Pearl River was at flood stage during most of the experiment and tidal influences were overwhelmed by river discharge. Fig. 3 shows river stage at the nearest USGS gauging station (02489500), upstream at Bogalusa, LA. The experimental period is highlighted in gray and the flood stage at that gauge is indicated.

A Teledyne RD Instruments (RDI) 1,200-kHz, four-beam acoustic Doppler current profiler (ADCP) was deployed on a heavy pyramidal bottom mount frame in the main channel of the lower east Pearl River at 30°19′54″ N, 89°37′52″ W. It was located in the thalweg, initially in 7 m of water (see Figs. 1 and 2). Two boats and crews were employed to ensure that the 1-2 beam pair was aligned with the dominant axis of the flow. The ADCP operated in burst mode pinging at 2 Hz for 5-min (600 pings) every half hour and logged every ping in beam coordinate mode with 0.25-m-deep bins. The sample interval and ensemble time were dictated by data storage concerns. Accounting for frame height and blanking distance, the first bin was centered 1.5 m above bottom. The 1-2 beam pair was aligned along the main axis of the channel.

Compass and pitch and roll sensors show that during this deployment the instrument's heading changed less than 1° over

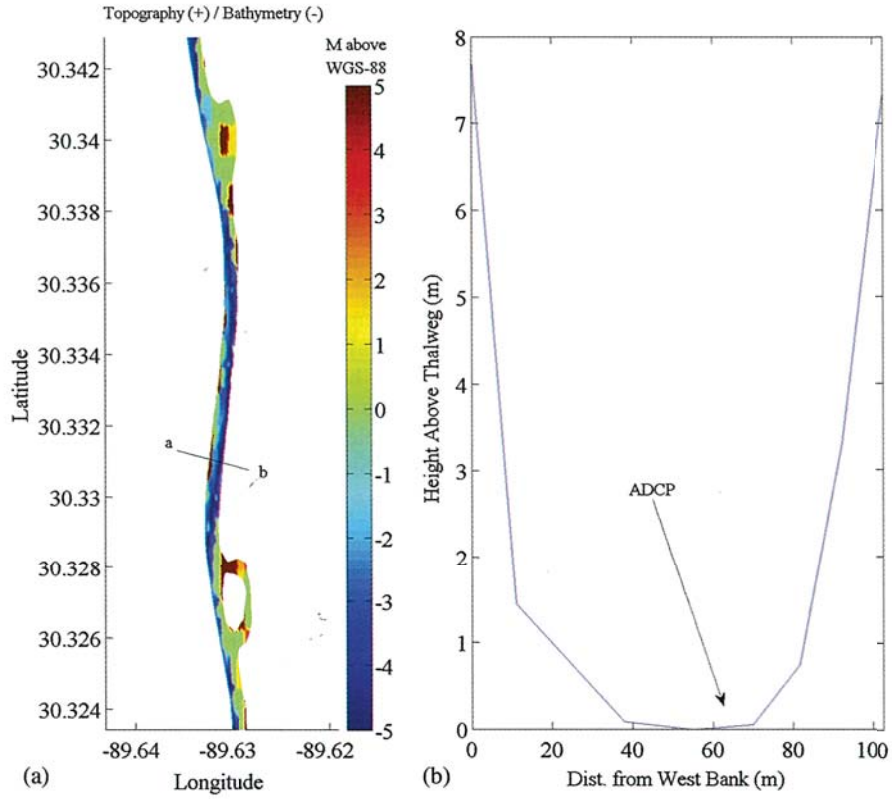

Fig. 2. (Color) Bathymetric map of a reach of the upper east Pearl River from multibeam acoustic surveys; the mooring location and cross section are indicated; river channel bathymetry at the mooring location viewed as looking downstream is on the right; positive x is along channel downstream, and positive y is to the right of that; $Y = 0$ is the left (east) bank; the mooring location is indicated

30 days, with most of that change occurring rapidly on Year Day (YD) 42. Pitch and roll started out at 0.7° and 2.7°, respectively, from the vertical with both changing slightly on YD 42 and then holding at 0.4° and 3.8°, respectively. It is likely that the mooring was bumped by an object moving along the river bed on YD 42. Even though stress estimates are very sensitive to instrument alignment with the vertical, Lu and Lueck (1999) showed that errors in the stress estimate will be small for such small deviations. The coordinate system is aligned such that x is the along channel direction, positive towars the ocean; y is the cross channel direction, to the right of x; and z is the vertical direction, positive down.

Working in beam coordinates, for each beam, and each ping the velocity data in the top two and bottom two bins was removed to eliminate both surface noise and ringing near the transducer head. Each beam was further cleaned by removing all data with a percent good (PG) of less than 90% as reported by the internal diagnostics of the ADCP. This removed a small number of bins, less than 1% of the data, with low echo strength. Removed data were replaced by interpolation between the bins above and below. Finally, for each burst, the data in each bin were cleaned by removing any value more than two standard deviations away from the ensemble average at that bin and replacing it with an interpolated value.

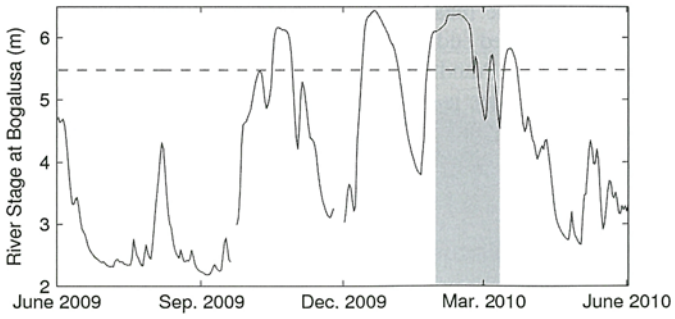

Fig. 3. River stage at the nearest upstream gauging station (Bogalusa, LA—02489500) for 6/1/2009–6/1/2010; the deployment period is highlighted in gray; flood stage at Bogalusa (5.5 m) is indicated by the dashed line

The along channel (u) and cross channel (v) velocities were calculated from the individual ADCP pings

$$u = \frac{B_2 - B_1}{2 \sin\theta} \tag{1}$$

$$v = \frac{B_4 - B_3}{2 \sin\theta} \tag{2}$$

where B_i = the along beam velocity for each beam ($i = 1, 2, 3, 4$), the 1-2 beam pair is aligned with the channel, the 3-4 beam pair is aligned cross-channel, and $\theta = 20°$ is the beam angle (for the RDI ADCP used) (Di Iorio and Gargett 2005). The instantaneous u and v velocities at each bin were then averaged for each 5-min burst to get the mean flow.

The variance method (which will be described later) requires that one beam pair, in this case the 1-2 beam pair, must be aligned along the dominant axis of flow. This was verified by comparing the u (from pair 1-2) and v (from pair 3-4) velocities, which clearly demonstrated that the u velocities were along the flow axis.

Two Seabird SBE-37SM microcat conductivity-temperature (CT) meters were deployed at the mooring, one mounted to the

mooring frame itself and the other suspended 1 m below a surface float. These measured temperature and salinity (zero in these waters) every 15 min with clocks synched to the ADCP. Water depth was taken from the pressure sensor on the ADCP.

Estimation of Vertical Mixing

In a sheared flow, vertical mixing results from both internally generated turbulence and turbulence generated by friction and stress at the top and bottom boundaries. Abraham (1980) showed that in a well-mixed system, as the Pearl will be shown to be, bottom boundary turbulence is dominant with maximum mixing occurring near the bottom and extending upward into the water column.

Turbulent mixing is commonly treated as a gradient process parameterized against the mean velocity shear with a turbulent eddy viscosity, K_m, and scalar diffusivity, K_s respectively, (with units of $m^2\ s^{-1}$) such that

$$-\overline{u'w'} = K_m \frac{\partial \bar{u}}{\partial z} \tag{3}$$

$$-\overline{w's'} = K_s \frac{\partial \bar{s}}{\partial z} \tag{4}$$

where the along channel and vertical velocities are u and w, respectively; the subscripts m and s imply diffusion of momentum and scalars (such as heat, sediment or any other passive tracer), respectively; an overline represents a time averaged quantity; and primed values represent the turbulent fluctuations from the time average (Dyer 1997).

Since the early 1990s, it has become common to estimate vertical eddy viscosity, or momentum diffusivity, using a pulse coherent four-beam, high-frequency broadband acoustic Doppler current profiler (ADCP). This method, known as the variance method, is based on the work of Lohrman et al. (1990), as elaborated by Stacey et al. (1999a, b) and Lu and Lueck (1999), and allows the direct estimation of the Reynolds stress, $\tau_x/\rho = -\overline{u'w'}$, by comparing the velocity variances of opposing pairs of beams. This stress is determined using the relation

$$-\overline{u'w'} = \frac{\bar{B}_{2f}^2 - \bar{B}_{1f}^2}{2 \sin 2\theta} \tag{5}$$

where $\bar{B}_{1f}^2 = \bar{B}_1^2 - \bar{B}_1{}^2$, B_1 is the velocity along the beam 1 direction, and the subscript f implies fluctuations (Di Iorio and Gargett 2005). $\bar{B}_{2f}^2$ is similarly defined but opposite from beam 1. The time-varying stress can then be estimated throughout the water column and parameterized against the observed vertical velocity gradient and thus K_m can be estimated using Eq. (3).

Energetic rivers often are vertically well mixed and thus have a gradient Richardson number close to zero. In such situations Stacey et al. (1999a) showed that the turbulent Prandtl number (K_m/K_s) approaches 1 as there is no stratification to resist the vertical transfer of either momentum or scalar properties.

Since the four beams of the ADCP spread apart from each other as they radiate upward, the variance method requires that the flow is horizontally homogeneous such that there is no variation in the turbulent statistics over the separation distance between corresponding bins in each beam pair (Lu and Lueck 1999). This condition is met by the deployment location being in the middle of the channel in a region of nearly constant cross section along channel. With the sampling rate of 2 Hz and vertical bin size of 0.25 m, the smaller eddies in the flow, which are involved in vertical momentum transfer (Rippeth et al. 2002), could be resolved. The 5-min ensemble time represents a compromise between concerns of instrument battery life, the need for a statistically significant sample size, and the need for quasi-stationary conditions during the sample period. With a 2-Hz sampling rate, a 5-min sampling period (600 samples) provides a statistically significant ensemble average of the velocity as the estimated standard error was low (less than 1 cm/s). In a flow dominated by quasi-steady river flux and lunar diurnal tides, the 5-min period was short enough to ensure quasi-stationary conditions during the entire ensemble.

Stress profiles were calculated for each ping in the record and then averaged for each 5-min ensemble to give one stress profile for each half hour period. The statistical reliability of the Reynolds stress estimates increases with the square root of the number of samples per ensemble according to the relation given by Williams and Simpson (2004)

$$\sigma_R^2 = \frac{\gamma(\sigma_n^2 - \langle B_{if}^2 \rangle)^2}{N \sin^2 2\theta} \tag{6}$$

where σ_R^2 = the mean squared variability of the Reynolds stress estimate, γ = a factor depending on the covariance of the individual velocity values, σ_n = the instrument noise level, $\langle B_{if}^2 \rangle$ = the mean square value of the turbulent fluctuations, and N = the number of samples per ensemble. From Eq. (6) and following the method of Williams and Simpson (2004), a threshold value for detectable stress can be estimated by examining low flow, when B_{if} goes to zero and γ to one, and taking a value for instrument noise of $\sigma_n = 0.017\ m\ s^{-1}$ from the instrument manufacturer. This then gives an approximate theoretical minimum measurable stress $\tau/\rho = 2 \times 10^{-5}\ m^2\ s^{-2}$. This is, as will be seen, an order of magnitude below the measured stresses.

To estimate the vertical eddy viscosity, K_m, it is necessary to parameterize $-\overline{u'w'}$ against the vertical shear in the along channel velocity, $\partial \bar{u}/\partial z$, in the region where stresses are resolved by the ADCP. As small variations in $\bar{u}$ between depth bins can cause large swings in the value of $\partial \bar{u}/\partial z$, as calculated using numerical differentiation techniques, each velocity profile was smoothed by fitting with a log curve and the gradient taken by differentiating that curve.

Vertical mixing time during the tidal cycle can be estimated from low-pass filtered values for a depth averaged vertical mixing quantity K_s (Lewis 1997), such that K_s is considered quasi-stationary, as

$$t = \frac{H^2}{8\bar{\bar{K}}_s} \tag{7}$$

where t = the approximate time for complete vertical mixing (in seconds), H = the mean water depth, and $\bar{\bar{K}}_s$ = the long period and depth averaged eddy diffusivity estimated from eddy viscosity using a turbulent Prandtl scaling of 1 such that $K_s = K_m$. This estimated mixing time is based on the estimated time required for a concentrated substance in the middle of the water column to assume a Gaussian concentration distribution with depth.

Results and Discussion

Although it is apparent in Fig. 3 that the Pearl River crossed flood stage at Bogalusa shortly before the beginning of the experiment, the flood wave did not reach the study site until approximately 2 days later [see Fig. 4(c)]. The water continued to rise at the study site until cresting on YD 42 and then began to decrease as the flood passed. While the tidal signal is visible at all times, significant tidal

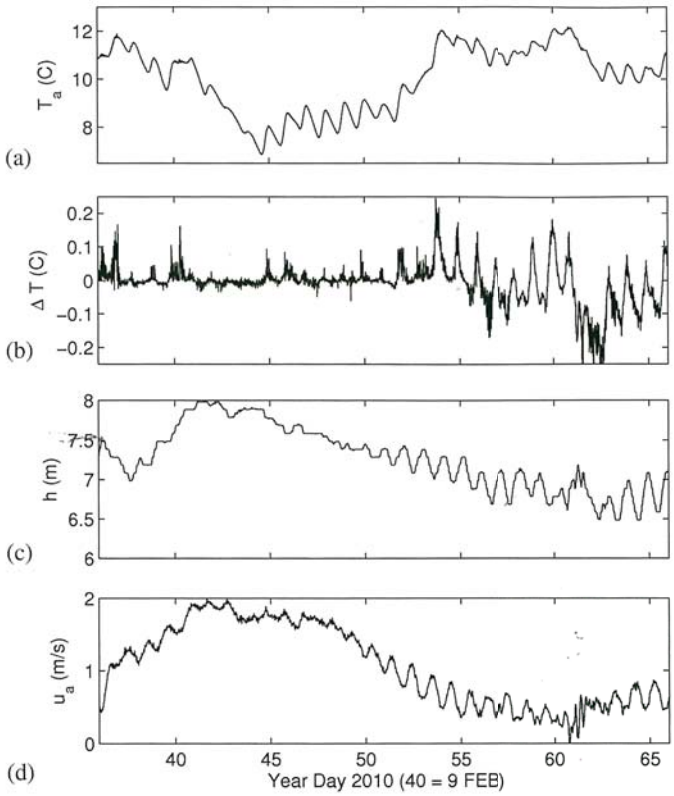

Fig. 4. (a) Depth-averaged temperature; (b) surface to bottom temperature difference; (c) water depth; (d) depth averaged along channel velocity at the mooring

depth variation began to be apparent again around YD 50 with the range increasing as the flood continued to ease.

Mean Flow and Stratification

Given a lack of information about how the temperature varies from the surface to the bottom, it has been assumed to vary linearly. Thus the depth-averaged temperature, defined as $T_a = 1/h\int_{-h}^{0} T(z)dz$, is given by the simple mean of the surface and bottom temperatures. The depth-averaged velocity is taken from the measured profile as $u_a = 1/h\int_{-h}^{0} u(z)dz$, where h is the time-varying water depth.

The depth-averaged temperature is shown in Fig. 4(a), and the surface to bottom temperature difference ($\Delta T = T_0 - T_{-h}$) is shown in Fig. 4(b). Although there is some diurnal surface heating and cooling due to atmospheric influences, particularly during the period of lower flow after YD 50, the difference over the depth of the water column, shown Fig. 4(b) with depth shown in Fig. 4(c), is low enough that the water column can be considered essentially vertically well mixed at all times.

Fig. 4(d) shows the depth averaged along channel velocity (u_a). Due to the high discharge rate, the velocity is always positive, flowing seawards, but a lunar diurnal signal is seen as the tides oppose, and attenuate, the discharge on flood tide. The flow stops and comes to near zero on YD 61 as discharge briefly drops too low to oppose the tide before it picks up again at the end of the experiment as discharge again increases.

Stress Production

The time and depth-varying profiles of the along channel velocity (u) is shown in Fig. 5(a) and of the turbulent stress ($-\overline{u'w'}$) in

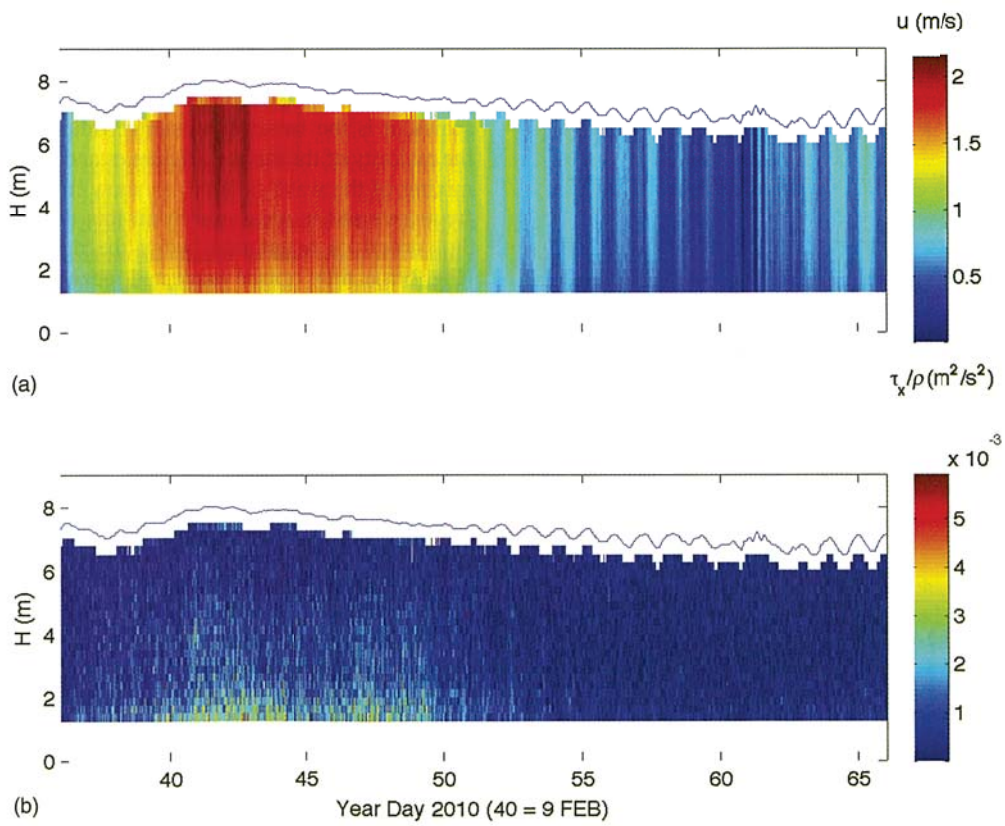

Fig. 5. (Color) Profiles through the experiment of (a) the along channel velocity, u; (b) the turbulent stresses, $-\overline{u'w'}$

Fig. 5(b). The no-slip condition at the bed requires that velocities rise rapidly from zero in the lower layers of the water column. They reach their maximum in the mid water column and stay constant with depth to satisfy the no-shear condition at the free surface.

Fig. 5(b) shows the stress ($\tau_x/\rho = -\overline{u'w'}$) through the water column. As predicted by Abraham (1980), maximum stresses originate near the bed and propagate upwards into the water column decreasing in the upper layers. The periods of highest stress are found during the peak of the flood when stresses reach as high as 5.5×10^{-3} m^2 s^{-2} near the bed and penetrate high into the water column, having a minimum around 1×10^{-3} m^2 s^{-2} near the surface. Stress magnitude drops off rapidly as the flood passes and velocities decrease. As along channel velocities briefly drop to near zero in the face of the incoming tide, bottom-generated stresses cease to dominate, and the stresses become low and patchy as internally generated turbulence, due to velocity shear in the water column, briefly dominates.

Fig. 6(a) shows a time series of τ_x/ρ in the lowest good bin, centered 1.5 m above bottom (MAB), for the entire deployment period. Maximum stresses are seen to be generated around the time of the maximum flood, and there is significant high- and low-frequency variability in the signal with peak positive and negative stresses on the order of 5×10^{-4} m^2/s^2. Low-pass filtering with a 40-h, third-order Butterworth filter removes tidal and higher frequencies from the signal (Emery and Thompson 2004). Lower-frequency tidal components will be negligible in such a short record (Pugh 2004). This is shown in Fig. 6(b). Stresses can be seen to track the river discharge peaking around YD 44–45 at 2.5×10^{-4} m^2/s^2 and then decreasing to near zero as the flood wave passes.

Tidal modulation of flow is evident through the entire deployment period with its importance increasing as river discharge decreases. Subtracting the low-frequency stress component in Fig. 6(b) from the full signal in Fig. 6(a) isolates the stress components at tidal frequencies and higher. Filtering that signal with a 4-h, third-order Butterworth filter isolates the tidal component with frequencies of M6 or lower, which is shown in Fig. 6(c).

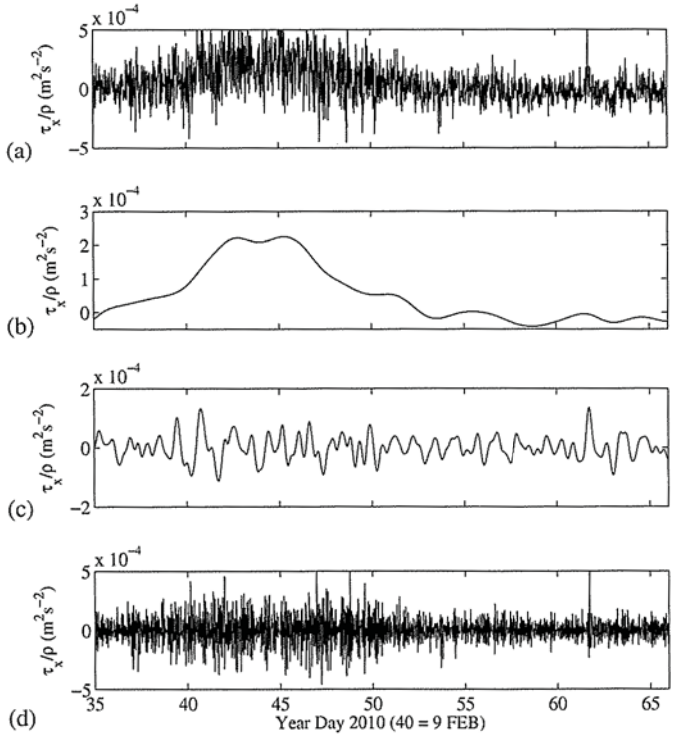

Fig. 6. Measured turbulent stress at 1.5 m above bottom for (a) the entire experiment; (b) stress due to river discharge; (c) tidal flows; (d) the residual

Tides in the central coast of the Gulf of Mexico show daily and fortnightly modulation with each lunar month exhibiting both a strong and a weak spring tide showing primary lunar diurnal tidal frequencies (24 h 50 min) and two uniformly weak neap tides showing primary lunar semidiurnal frequencies (12 h 25 min). A strong spring tide occurred around YD 40 with peak positive stress on ebb tide reaching as high as 90% of the discharge related stress. Stresses around this time show a pronounced ebb dominance with higher stresses on the shorter but stronger ebb and lower stresses on the longer but weaker flood. This flood/ebb asymmetry is a common feature of flows in tidal rivers and inlets and is caused by distortion of the tidal wave due to bottom friction (Blanton et al. 2002). The frequency is the primary lunar diurnal with very small semidiurnal signal evident as a slight modulation of the signal. Neap tide occurred 7 days later and was characterized by lower stresses and a lunar semidiurnal frequency with no particular ebb dominance observable. This is followed by a weak spring tide with stresses less than the previous spring tide and a slight ebb dominance. The final neap tide is identical to the previous.

The residual stresses are due to random instrument noise as well as high-frequency processes tied to surface wind stresses, residual flows and, in some cases, disturbances due to the passage of high speed boats (such as on YD 48) and may be obtained by subtracting the signals in Figs. 6(b and c) from Fig. 6(a). They are shown in Fig. 6(d). Even though the magnitude is larger than that of the stresses due to discharge or tidal processes, there is no discernible dominant frequency or positive or negative bias and the mean is near zero at 1.5×10^{-7} m^2/s^{-2}). They are thus unlikely to contribute significantly to vertical mixing.

Not addressed in these measurements are small-scale, high-frequency stresses that are outside of the measurement range of the ADCP used. While these stresses are important to local mixing and in transferring turbulent kinetic energy down to dissipative scales, it is the larger dominating eddies that are responsible for the majority of the mixing (Tennekes and Lumley 1999) and for the mixing of the water column, as show in Fig. 7. Since the highest frequency eddies measured by in this deployment [Fig. 6(d)] are 3–4 orders of magnitude below the dominant frequency eddies [Fig. 6(a)], they can be neglected when addressing water column mixing processes.

Nonlinear least squares regression analysis was performed comparing the discharge and tidal stresses to the measured total stress to compute an r^2 value that expresses the degree to which the measured signal is accounted for by each individual component. The discharge generated stresses in Fig. 6(b) fit the total stress in Fig. 6(a) with an $r^2 = 0.41$ indicating that they contribute somewhat less than half of the total near bed stress during the entire deployment period. Similarly, the tidal stresses in Fig. 6(c) fit the total stress with an $r^2 = 0.51$, contributing slightly over half of the stress during the deployment.

Dividing the deployment period into two sections, a high discharge period before YD 52 and a tidally dominated period after YD 52 and repeating the analysis shows that during the high discharge period the discharge-related stresses fit the total stresses with an $r^2 = 0.68$ while the tidal stress' fit is reduced to an $r^2 = 0.29$. Conversely, in the lower discharge period, the discharge-related stresses fit the signal with an $r^2 = 0.21$, whereas the tidal stresses fit with an $r^2 = 0.77$. This clearly shows the exchange between discharge and tidal flows in generating mixing

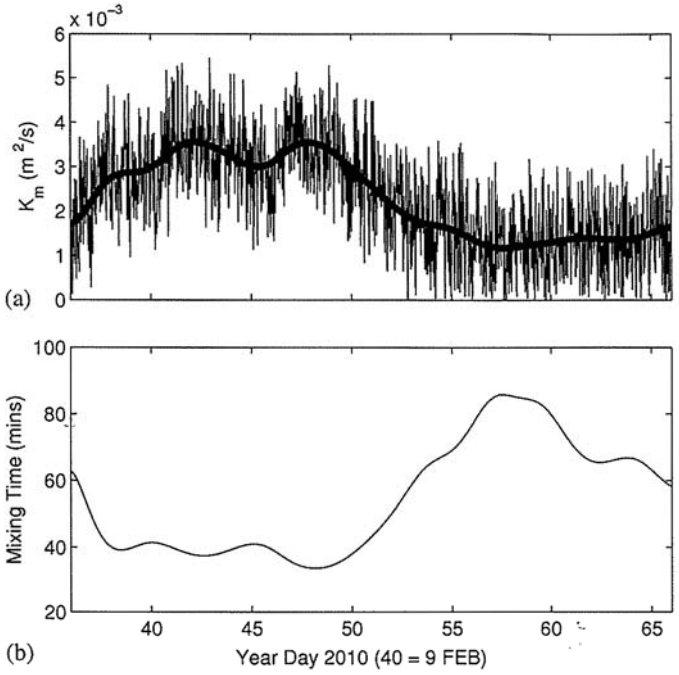

Fig. 7. (a) Depth-averaged vertical eddy viscosity with the 40-h low-pass filtered value indicated by the heavy line; (b) the estimated vertical mixing time in minutes

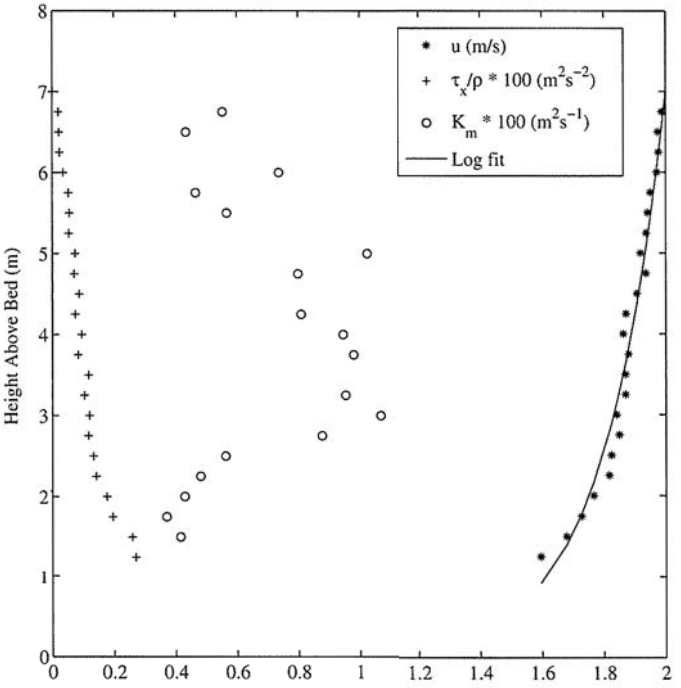

Fig. 8. Measured stresses at maximum discharge on YD 42 (plus signs); these are parameterized against the velocity profile (solid line) to calculate the vertical eddy viscosity, K_m, (open circle)

stresses as the discharge decreases and tidal flows begin to reestablish.

Vertical Eddy Viscosity

Vertical eddy viscosity, K_m, is calculated by parameterizing the stress, τ_x/ρ, against the vertical shear, $\partial\bar{u}/\partial z$ as shown in Eq. (3). Fig. 8 shows one stress profile (indicated by +) on YD 42, during the time of maximum flood velocity. The stresses are greatest near the bed and decrease nearly linearly with height above bed. The stresses are parameterized against the shear in the velocity profile (indicated by the * with a log fit shown by the solid line) to calculate the vertical eddy viscosity K_m. This is shown with the open circles. Even though there is some spread to this term, it broadly shows the parabolic distribution with depth which is typical in shallow water flows (Jobson and Sayre 1970), with a maximum in the midwater column where shear goes low but stresses are still high.

Fig. 9 depicts the same profiles during the incoming flood tide on YD 60, during a low-discharge period when tidal flows were being reestablished. Velocities are lower by a factor of approximately 5 with the profile showing greater shear as discharge and tidal flows oppose each other. Stresses are an order of magnitude lower but penetrate further into the water column, due to the greater importance of shear in the flow compared to bottom stress. This results in a vertical mixing profile that still shows a parabolic form but has greater variability and spread.

As substances mix through the water column they experience the entire vertical range of mixing energy. This range can be parameterized as an effective depth averaged $\hat{K}_s$. Since the system is well mixed, this $\hat{K}_s$ can be approximated as $\hat{K}_m$, which is shown in Fig. 7(a). The mean value of $\hat{K}_m$, shown by the heavy line as a 40-h low-pass filtered value, varies with flood stage and river discharge, as has been previously noted, representing different levels of vertical mixing. Even the low values, however, represent strong vertical mixing in this shallow system (Lewis 1997).

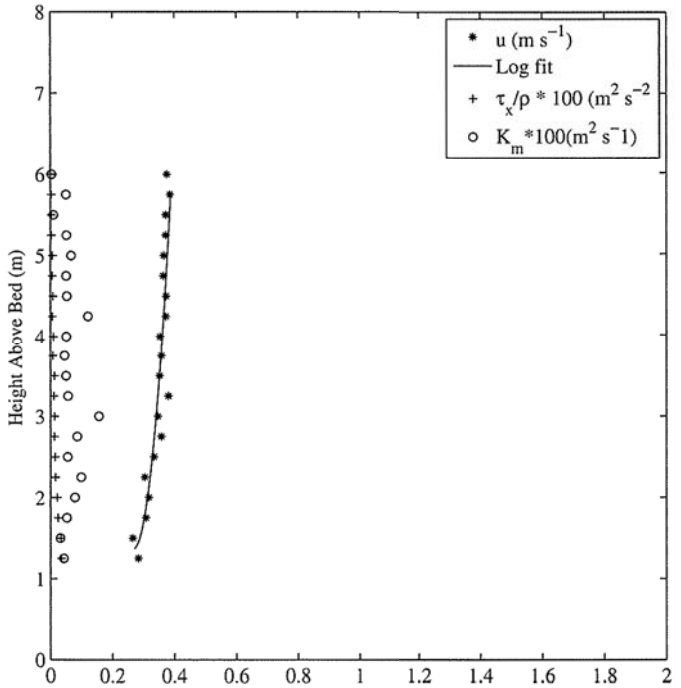

Fig. 9. Measured stresses at low discharge on a flood tide on YD 60 (plus signs); these are parameterized against the velocity profile (solid line) to calculate the vertical eddy viscosity, K_m, (open circle)

Eq. (7) facilitated calculation of the approximate time for complete vertical mixing as a function of the mean water depth and the mean, depth averaged value of K_z. This is shown in Fig. 7(b) plotted in minutes. Even at its slowest, complete vertical mixing is achieved in slightly over 1 h, 20 min and at maximum discharge

takes as little as 35 min. As even the larger of these two numbers is very much less than the diurnal period of the atmospheric and tidal influences which serve to induce stratification, it is likely that the Pearl River stays vertically well mixed during all similar conditions.

Turbulent Parameterizations

In modeling river flows, it is generally not possible to directly model the turbulent flows so some simplified parameterization must be employed to achieve turbulence closure and thus to be able to predict the vertical mixing in the flow. One simple method is to employ Prandtl's mixing length model. Prandtl hypothesized that for simple wall bounded flows, the vertical eddy viscosity, shown in Eq. (3) as K_m, can be parameterized as

$$K_m = \left|\frac{\partial \bar{u}}{\partial z}\right| \ell_m^2 \tag{8}$$

where ℓ_m = the mixing length, a parameter that varies spatially through the flow and temporally as velocity shear changes with flow conditions. Substituting in Eq. (3) and rearranging, the mixing length can be expressed as

$$\ell_m = \left(\frac{-\overline{u'w'}}{\left|\frac{\partial \bar{u}}{\partial z}\right|\frac{\partial \bar{u}}{\partial z}}\right)^{1/2} \tag{9}$$

Calculating this mixing length for all bins at all times during the experiment shows very little variation of mixing length with depth. Fig. 10 shows the instantaneous depth-averaged mixing length for the entire deployment. The heavy line indicates a 40-h low-pass filtered value that eliminates tidal and higher-frequency variability. The mixing length is seen to be lower during the first part of the experiment when bottom stresses dominate and stress drops rapidly with height above bed. As discharge decreases in the second half of the deployment and tidal flows begin to reestablish, the mixing length increases as time-averaged bottom stresses decrease due to the tidally oscillating nature of the flow at a greater rate than the similar decrease in vertical mixing stresses.

Fischer et al. (1979) showed that for fully developed, turbulent, open channel flows, the vertical eddy viscosity (K_m) can be represented as

$$K_m = \kappa d u_* \left(\frac{z}{d}\right)\left[1 - \left(\frac{z}{d}\right)\right] \tag{10}$$

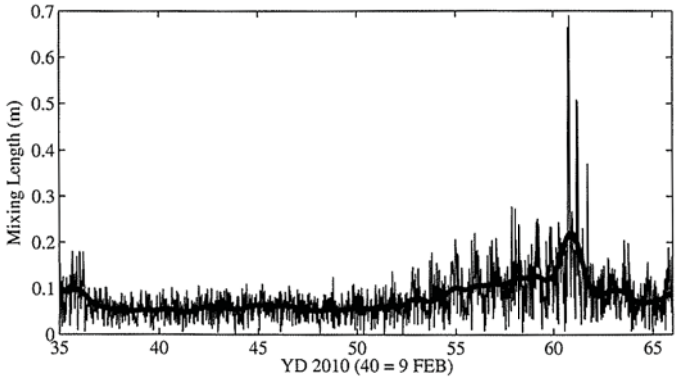

Fig. 10. Depth averaged mixing length (ℓ_m) with the 40-h low-passed value indicated by the heavy line

where κ = the von Karman constant (taken here to be 0.4), d = the river depth, z = the height above bed, and u^* = the friction velocity defined as $u^* = \sqrt{\tau/\rho}$ with τ being the bottom stress and ρ the fluid density. Experimental work by Jobson and Sayre (1970) showed that the same formulation can work for vertical eddy diffusivity in cases where the Prandtl number approaches 1 and that it is generally accurate to within 25% in rivers.

Examining the vertical structure of Eq. (10) in Fig. 11, a generally good agreement with the vertical structure of measured K_m and Fischer's predictions at both high and low flows can be seen. At high flows, Fischer's model correctly predicts peak, mid water column, stresses but overpredicts stresses above and below that level but as much as 20%. Agreement is somewhat better at low flows with differences being generally less than 15%.

Depth averaging Eq. (10), it can be shown that

$$K_m = 0.067 d u_* \tag{11}$$

Fig. 12(a) shows the instantaneous depth-averaged values for K_m as calculated using Eq. (11) in blue and as measured in red. Fig. 12(b) compares the 40-h low-pass filtered versions of the same quantities. The calculated instantaneous signal shows somewhat greater variability than the directly measured signal but shows a similar form. Examining the low-pass filtered signals, the calculated eddy viscosity compares well in trend to the measured signal but is at all times greater, varying between 10 and 50% higher. This compares well with the predictions from examining the vertical structure. This consistent difference suggests that the formulation of Csandy (1976), where the coefficient in Eq. (11) was measured to be 0.05 in the atmospheric boundary layer, may be more appropriate as it will slightly lower the prediction.

In this work, the common convention in tidally dominated estuarine flows of treating the bottom 1.5 m of the flow as being essentially a constant stress layer has been employed. To address the possibility of this introducing errors into calculations of both of

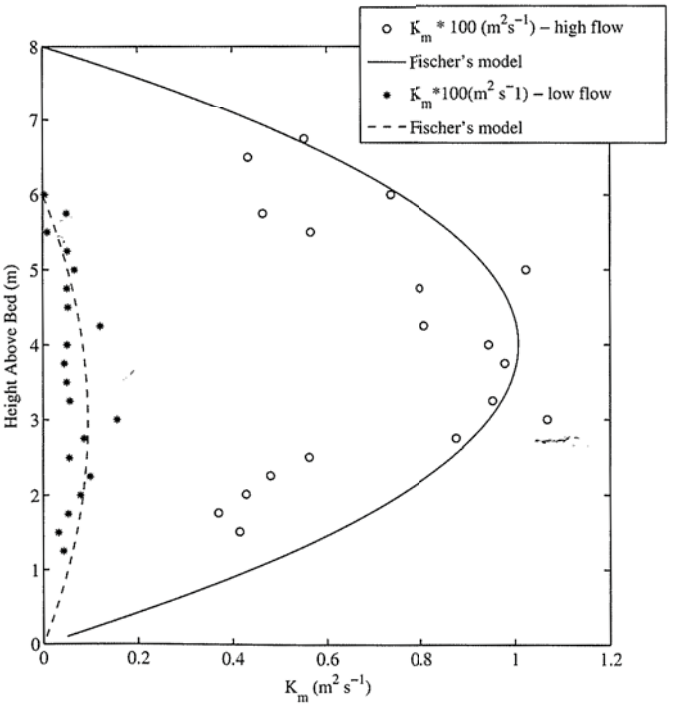

Fig. 11. Vertical profiles of K_m from Figs. 7 and 8 plotted with Fischer's model for the vertical structure of K_m

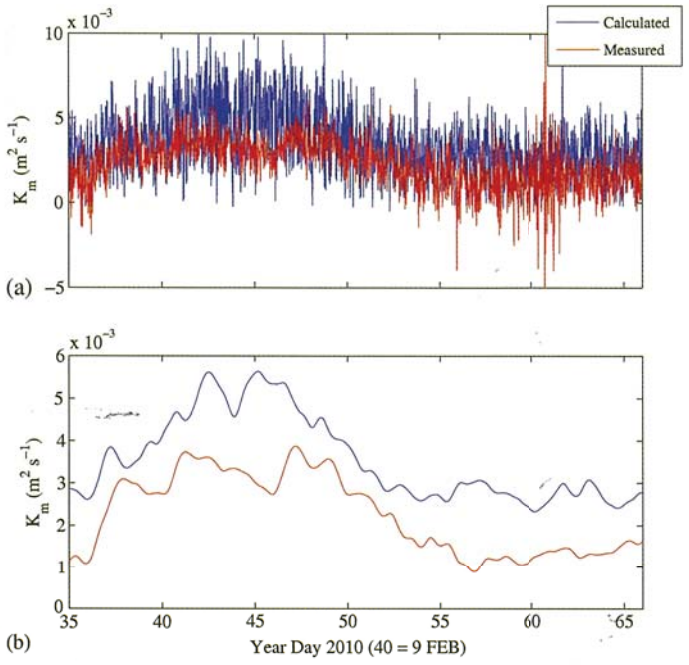

Fig. 12. (Color) (a) Instantaneous values of K_m is calculated using Eq. (11) (blue) and from measured stresses (red); (b) 40-h low-pass filtered versions of the same quantities

the depth average of K_m and of u^*, each stress profile to the bed has been extrapolated to more properly estimate bed stress. At times of high discharge-dominated flows during the early part of the deployment, this increased the estimated bed stress by as much as 30%; however, during times of low or tidally dominated flow, the bed stress estimates only increased by 2–4%. Averaged across the entire deployment, this results in a mean increase in bed stress estimates of 6%. As this increase applies only at the bed and decreases rapidly above bed until merging with the measured stresses at 1.5 MAB, the effect on the depth-averaged value of the measured K_m is negligible, representing an increase of 0.1%. The value as calculated using Eq. (11) increases in accord with the increase in estimated bed stress, between 2 and 30% with a mean increase of 6%. Due to the uncertainty inherent in extrapolating the stress profiles to bed and the small effect on the results, it is believed that the assumption of a constant stress layer below the lowest measured bin is validated.

Conclusion

Measurements of currents and stresses in a shallow coastal plain river during a minor flood event and the beginning of the reestablishment of tidally dominated flow have been presented. These measurements directly resolve the vertical velocity structure through the water column as well as allow the estimation, through the variance method, of the turbulent stresses that give rise to the vertical mixing of momentum and scalars. Spanning a 30-day period, these measurements cover the peak of river discharge and the transition back to the normal tidally dominated regime of this river. As a result, a wide range of time scales from turbulent to tidal to synoptic weather scales (as the discharge is driven by rainfall runoff) could be resolved.

The river stayed well mixed at all times owing to the energetic nature of the flows due both to river discharge and tidal flows. Due to this, the Prandtl number can be assumed to be near 1 and the vertical eddy viscosity and diffusivity to be nearly equal.

Estimates of the vertical turbulent stress, τ_x/ρ, show stresses generated near the bed and penetrating high into the water column. Times of maximum stress generation are tied to the strong currents associated with flooding conditions. As discharge drops and tidal flows are reestablished, stresses are still generated at the bed but shear in the water column, and internally generated turbulence take on a greater role in mixing. Decomposition of these stresses into their discharge-related and tidally driven components establishes the importance of tidally driven mixing even during high discharge periods where tidal influences are not readily visible in the data. High-frequency stress fluctuations are much larger than the sustained stresses due to river flows, but as they average to nearly zero and show no bias in sign, they will not contribute greatly to vertical mixing, thus confirming that it is the large, lower frequency eddies that do much of the work in mixing the water column.

Measured stresses through the water column show peaks near the bed with stresses rapidly decreasing with height above the bed. In the more energetic discharge-dominated flows typical of the beginning of the deployment, these stresses decrease rapidly with height above bed; during less energetic flow toward the end of the experiment, the stresses are an order of magnitude less but penetrate further into the water column. This is likely due to the increased importance of shear in the velocity profile as compared to bed stressed at these lower speeds, where tidal oscillations attenuate flows, which serves to generate internal turbulence to supplement the bottom-generated turbulence. This results in a more uniform distribution of stresses through the water column at low flows than at high flows when bottom stress dominates.

Vertical eddy viscosity (and by extension in these well mixed waters, eddy diffusivity) shows a classic parabolic form with respect to depth during high flow times with a similar but more noisy profile, though still parabolic, during lower flow times. At all times, the vertical mixing is sufficient to mix the water column on time scales much faster than the semidiurnal, diurnal, and slower scales of forcing variability. The more energetic flows at the beginning of the experiment mix the water column in approximately 40 min, whereas the slower and more tidal flows at the end take twice as long. Both regimes are, however, capable of keeping the water column well mixed at all times.

Prandtl's mixing length model is used to show the relative contributions of unidirectional and tidal flows on mixing length. In contrast to classical theory, which holds that mixing length is directly tied to water depth, these measurements indicate that tidal oscillations in flow increase mixing length, despite a decrease in channel depth, due to a decrease in bottom shear when averaged over tidal time scales.

An alternate method of parameterizing mixing, using Fischer et al. (1979) observations of open channel flows, enabled the prediction of the form and magnitude of the vertical eddy viscosity using friction velocity, a common input in models based on bed composition. This shows good agreement with measured values of eddy viscosity but is slightly biased high. Errors are low during the energetic periods of flow but become significant as flow decreases indicating that a slightly tweaked model might be more appropriate in these lower mixing periods. Either method, however, is sufficient to estimate vertical mixing in the river with enough fidelity for most modeling efforts.

The work then shows how vertical mixing in rivers, driven by bed stresses and velocity shear, keeps energetic rivers well mixed whether dominated by tidal flows or river discharge. The oscillating nature of tidal flows reduces mean shear while allowing a more uniform distribution of stresses through the water column. Higher,

one-directional, discharge-dominated flows enhance both bottom stress and shear allowing more energetic mixing. In the absence of any salinity or temperature-based stratification, the river will stay essentially well mixed at all times with the mixing largely due to low-frequency eddies with length scales on par with the river depth.

Acknowledgments

This work was supported under the NRL 6.2 Core Project "The Performance of a Persistent Riverine Surveillance Network." The authors thank Dr. Alan Weideman, Dr. Bill Teague, Mr. Wesley Goode, and Mr. Mark Hulburt for their valuable help with the experimental program. The authors further thank the editor and the three anonymous reviewers for comments which have made this a much improved paper. This paper is NRL contribution number NRL/JA/7320-10-0484.

References

Abraham, G. (1980). "On internally generated estuarine turbulence." *Second Int. Symp. on Stratified Flows*, T. Carstens and T. McClimans, eds., AIHR, Delft, Netherlands, 344–363.

Blanton, J., Lin, G., and Elston, S. (2002). "Tidal current asymmetry in shallow estuaries and tidal creeks." *Cont. Shelf Res.*, 22(11–13), 1731–1743.

Chant, R. (2002). "Secondary circulation in a region of flow curvature: Relationship with tidal forcing and river discharge." *J. Geophys. Res.*, 107(C9), 3131–3142.

Chant, R., Geyer, R., Houghton, R., Hunter, E., and Lerczak, J. (2007). "Estuarine boundary layer mixing processes: Insights from dye experiments." *J. Phys. Oceanogr.*, 37, 1859–1877.

Csandy, G. (1976). "Mean circulation in shallow seas." *J. Geophys. Res.*, 81(30), 5389–5399.

Di Iorio, D., and Gargett, A. (2005). *Sounds in the sea: From ocean acoustics to acoustical oceanography*, Cambridge University Press, Cambridge, U.K., 500–517.

Dyer, K. R. (1997). *Estuaries: A physical introduction*, John Wiley and Sons, Hoboken, NJ.

Emery, W., and Thompson, R. (2004). *Data analysis methods in physical oceanography*, 2nd and revised Ed., Elsevier, Amsterdam, Netherlands.

Fischer, H., List, E., Koh, R., Imberger, J., and Brooks, N. (1979). *Mixing in inland and coastal waters*, Academic Press, Waltham, MA.

Fritz, H., et al. (2007). "Hurricane Katrina storm surge distribution and field observations on the Mississippi Barrier Islands." *Estuar. Coast. Shelf Sci.*, 74(1–2), 12–20.

Hansen, D., and Rattray, M. (1965). "Gravitational circulation in straits and estuaries." *J. Marine Res.*, 23, 104–122.

Jobson, H., and Sayre, W. (1970). "Vertical transfer in open channel flow." *J. Hydr. Div.*, 96(3), 703–724.

Lewis, R. (1997). *Dispersion in estuaries and coastal waters*, John Wiley and Sons, Hoboken, NJ.

Liu, H., Wu, C., Xu, W., and Wu, J. (2009). "Contrasts between estuarine and river systems in near-bed turbulent flows in the Zhujiang (Pearl River) Estuary, China." *Estuar. Coast. Shelf Sci.*, 83(4), 591–601.

Lohrman, A., Hackett, B., and Roed, L. (1990). "High resolution measurements of turbulence, velocity, and stress using a pulse-to-pulse coherent SONAR." *J. Atmos. Oceanic Technol.*, 7(1), 19–37.

Lu, Y., and Lueck, R. (1999). "Using a broadband ADCP in a tidal channel. Part II:Turbulence." *J. Atmos. Oceanic Technol.*, 16(11), 1568–1579.

Muste, M., Yu, K., Pratt, T., and Abraham, D. (2004). "Practical aspects of ADCP data use for quantification of mean river flow characteristics. Part 2: Fixed vessel measurements." *Flow Meas. Instrum.*, 15(1), 17–28.

Patrick, R. (1995). *Rivers of the United States. Volume II: Chemical and physical characteristics*, John Wiley and Sons, Hoboken, NJ.

Peters, H. (1997). "Observations of stratified turbulent mixing in an estuary: Neap-to-spring variations during high river flow." *Estuar. Coast. Shelf Sci.*, 45(1), 69–88.

Peters, H., and Johns, W. (2005). "Mixing and entrainment in the Red Sea outflow plume. Part II:Turbulence characteristics." *J. Phys. Oceanogr.*, 35(2), 584–600.

Piatt, H. (1982). "The Jackson flood of 1979: A public policy disaster." *J. Am. Plann. Assoc.*, 48(2), 219–231.

Pritchard, D. (1952). "Estuarine hydrography." *Adv. Geophys.*, 1, 242–280.

Pritchard, D. (1954). "A study of the salt balance in a coastal plain estuary." *J. Mar. Res.*, 13, 133–144.

Pugh, D. (2004). *Changing sea levels: Effects of tides, weather and climate*, Cambridge University Press, Cambridge, U.K.

Rippeth, T., Williams, E., and Simpson, J. (2002). "Reynolds stress and turbulent energy production in a tidal channel." *J. Phys. Oceanogr.*, 32, 1242–1251.

Shteinman, B., Merchaz, E., and Gutman, A. (1993). "Spatial structure of a jet flow at a river mouth." *Boundary-Layer Meteorol.*, 62(1–4), 379–383.

Simpson, J., Williams, E., Brasseur, L., and Brubaker, J. (2005). "The impact of tidal straining on the cycle of turbulence in a partially stratified estuary." *Con. Shelf Res.*, 25(1), 51–64.

Stacey, M., Monismith, S., and Burau, J. (1999a). "Measurements of Reynolds stress profiles in unstratified tidal flow." *J. Geophys. Res.*, 104(C5), 10933–10949.

Stacey, M., Monismith, S., and Burau, J. (1999b). "Observations of turbulence in a partially stratified estuary." *J. Phys. Oceanogr.*, 29(8), 1950–1970.

Stone, M., Tritico, H., Hotchkiss, R., and Flanagan, P. (2003). "Turbulence characteristics in obstructed gravel bed flow." *Proc., of the 16th ASCE Engineering Mechanics Conf.*, ASCE, Reston, VA.

Tennekes, H., and Lumley, J. L. (1999). *A first course in turbluence*, MIT Press, Cambridge, MA.

Thornbury, W. (1965). *Regional geomorphology of the United States*, John Wiley and Sons, Hoboken, NJ.

Turnipseed, D., Giese, G., Pearman, J., Farris, G., Krohn, M., and Sallenger, A., Jr. (1998). "Hurricane Georges: Headwaters flooding, storm surge, beach erosion and habitat destruction on the Central Gulf Coast." *Rep. No. 98-4231*, USGS Water Resources Investigations, Washington, DC.

Wax, C. (1990). "General climatology of Mississippi—Floods and droughts." *National water Summary 1988—Hydrologic Events and Floods and Droughts, USGS Water Supply Paper 2375*, USGS, Washington, DC.

Williams, E., and Simpson, J. (2004). "Uncertainties in estimates of Reynolds stress and TKE production rate using the ADCP variance method." *J. Atmos. Oceanic Technol.*, 21(2), 347–357.